Eur. Phys. J. D **14**, 205–215 (2001)

THE EUROPEAN PHYSICAL JOURNAL D

EDP Sciences

Ultrafast multidimensional dynamics of strong hydrogen bonds

A Cartesian reaction surface approach

G.K. Paramonov[a], H. Naundorf, and O. Kühn[b]

Institut für Chemie, Physikalische und Theoretische Chemie, Freie Universität Berlin, Takustr. 3, 14195 Berlin, Germany

Received 24 August 2000 and Received in final form 11 October 2000

Abstract. The laser driven dynamics of the OH(D) stretching vibration in phthalic acid monomethylester is investigated. The combination of a 55-dimensional all-Cartesian reaction surface Hamiltonian and the time-dependent self-consistent field approach is shown to provide a microscopic picture of intramolecular vibrational energy redistribution taking place upon interaction with an external laser field. Choosing suitable zeroth-order vibrational states and combinations thereof a quasi-periodic *in-phase* and *out-of-phase* oscillatory behavior is observed manifesting energy flow on different time scales. The fingerprints of this behavior in transient absorption spectroscopy are also discussed.

PACS. 33.15.Fm Bond strengths, dissociation energies – 31.15.Ar Ab initio calculations – 31.15.Qg Molecular dynamics and other numerical methods

1 Introduction

Multidimensional dynamics of coupled nuclear or vibronic degrees of freedom (DOF) in polyatomic molecules continues to be a challenge to both experiment and theory. On the experimental side it was appreciated already in the eighties that even rather large molecules, for which a high vibrational density of states is expected, can show a nonstatistical behavior. This is exemplified by the observation of quantum beats, for instance, in time-resolved fluorescence signals [1–4]. While this concerns the short time dynamics it has been shown that also the behavior on intermediate time scales is often far from being monoexponential [5] as would have been predicted by the classic Bixon-Jortner Golden rule approach [6] (for a recent review see also [7]).

From the theoretical point of view the concept of coupled zeroth-order states has been very fruitful in describing short time dynamics (for reviews see, *e.g.*, [7,8]). This is related to the fact that eigenstates of some multidimensional vibrational Hamiltonian, for instance, are hardly obtainable for large molecules. On the other hand, provided that the time scale related to the coupling between zeroth-order states is long compared to the duration of the laser pulse, zeroth-order states may be prepared in the experiment [9]. Establishing the link between theory and experiment, Felker and Zewail derived the conditions for observation of specific beating frequencies in coupled multilevel systems [10]. For two coupled zeroth-order states this gives the typical *in-phase* and *out-of-phase* oscillations of the state populations as a manifestation of the selectivity of energy flow (see also [11]) which have been observed, *e.g.*, in anthracene [3].

In the present contribution the ultrafast dynamics of the OH (and OD) stretching vibration in a strong intramolecular hydrogen bond formed in the electronic ground state is studied. Hydrogen atom and proton motion within hydrogen bonds is of outstanding importance for various processes in chemistry and biology [12–14]. Ultrafast proton transfer dynamics in the electronic excited state has already been observed for a number of molecular systems using time-resolved nonlinear spectroscopy [15–18] (for an overview about earlier work see also [19]). As a consequence of the large changes taking place in the electronic structure upon optical excitation, proton transfer can be strongly coupled to the molecule's low-frequency vibrations. This leads to vibrational coherences modulating the pump-probe signals [20,21].

Monitoring ultrafast hydrogen bond dynamics in the electronic ground state became feasible only recently with the development of intense femtosecond infrared (IR) laser sources. Among the topics which have been studied in this respect are, for instance, the dynamics of liquid water [22,23] or the OH-stretching dynamics of monomeric and dimerized alcohols [24]. Very recently, the group of Elsaesser reported on the observation of vibrational quantum beats after excitation of the OD and the OH-band, respectively, in phthalic acid monomethylester using 130 fs IR laser pulses in an IR pump-probe setup [25].

[a] *On leave from* National Academy of Sciences of Belarus, Institute of Physics, Skaryna Ave. 70, 220602 Minsk, Republic of Belarus.

[b] e-mail: `ok@chemie.fu-berlin.de`

These findings have been explained in terms of anharmonic couplings between the (nonreactive) OD dynamics and the low-frequency motion of the oxygen atoms which are involved in hydrogen bonding.

A microscopic modeling of the nuclear dynamics of polyatomics as induced by ultrashort IR laser pulses requires two ingredients: first, the Hamiltonian has to be defined. This can be done employing the reaction surface idea [26] where in particular the anharmonicity of the potential energy surface with respect to some selected coordinates is included (see Sect. 2.1). Second, given the multidimensional Hamiltonian an appropriate numerical method for the solution of the time-dependent Schrödinger equation has to be chosen. When using the reaction surface approach most of the nuclear DOF, *i.e.* the substrate or "bath", are treated in harmonic approximation. Thus a normal mode representation shall provide a useful zeroth-order reference although there is some coupling to the anharmonic coordinates as well as the possibility of mode-mode coupling (see Sect. 2.1). Having a Hamiltonian which suggests a separable representation of the different DOF, the time-dependent self-consistent field (TDSCF) approach [27] appears to be most suitable. Being based on a variational principle [28,29] it has the advantage that the numerical effort scales only linearly with the number of DOF (for a recent review see also [30]). In addition the harmonic treatment of the substrate facilitates an exact solution, *i.e.* these DOF behave like uncoupled linearly driven *classical* oscillators [31,32]. It has been pointed out, however, that in cases where the dynamics depend on details of the interaction potential between the separated DOF, a multi-configuration TDSCF treatment is required [32–34].

In the following we study the dynamics of a strong hydrogen bonded model system combining the reaction path Hamiltonian and the multidimensional TDSCF approach. In Section 2.1 the idea of the all-Cartesian reaction surface Hamiltonian is summarized. Its TDSCF implementation is discussed in Section 2.2. Numerical results are presented for phthalic acid monomethylester (PMME-H) and its isotope (PMME-D). This includes the analysis of the Hamiltonian in terms of strongly coupled modes in Section 3.1 and the laser driven dynamics in Section 3.2. In Section 4 we give a summary.

2 Theory

2.1 Cartesian reaction surface Hamiltonian

It has long being appreciated that proton or hydrogen atom dynamics can be strongly coupled to heavy atom motions of the molecular frame [35]. This necessitates the use of a multidimensional Hamiltonian for an adequate description of the molecular dynamics. Thus inspection of the minimum energy path, *i.e.* the intrinsic reaction coordinate [36], is not sufficient but orthogonal harmonic modes, for instance, have to be included along the reaction path [26,37]. For the case of proton transfer coupled to heavy atom motions the minimum energy path will be rather sharply curved such that it is more advisable to use a reaction surface defined in terms of several internal coordinates [38,39]. From the practical point of view this description has the disadvantage that the coupling between different DOF is contained in the kinetic energy operator. An alternative which is well-suited for proton transfer reactions as well as nonreactive proton motion in a strong hydrogen bond, is provided by an all-Cartesian reaction surface (CRS) Hamiltonian which contains all couplings in the potential energy operator [40]. A high-level quantum chemical realization of this concept for polyatomics has only recently been provided [41–43].

The first step in the construction of a CRS Hamiltonian is the identification of Cartesian large amplitude coordinates, $\mathbf{x}$, whose choice is often obvious in the case of hydrogen bond dynamics. The remaining coordinates are comprised into the substrate $\mathbf{Z}$, which is treated in harmonic approximation, similar to the case where internal reaction coordinates are used. Given a reference configuration $\mathbf{Z}^{(0)}$ of the substrate, *i.e.* usually the most stable geometry, the total potential energy surface (PES) is expanded in the vicinity of this reference configuration along the reaction surface:

$$U(\mathbf{x};\mathbf{Z}) \approx V_{\mathrm{ref}}(\mathbf{x}) + \left(\frac{\partial U(\mathbf{x};\mathbf{Z})}{\partial \mathbf{Z}}\right)_{\mathbf{Z}=\mathbf{Z}^{(0)}} (\mathbf{Z}-\mathbf{Z}^{(0)}) + \frac{1}{2}(\mathbf{Z}-\mathbf{Z}^{(0)}) \left(\frac{\partial^2 U(\mathbf{x};\mathbf{Z})}{\partial \mathbf{Z}\partial \mathbf{Z}}\right)_{\mathbf{Z}=\mathbf{Z}^{(0)}} (\mathbf{Z}-\mathbf{Z}^{(0)}) \quad (1)$$

where $V_{\mathrm{ref}}(\mathbf{x}) = V(\mathbf{x};\mathbf{Z}^{(0)})$. In a next step (mass-weighted) normal modes $\mathbf{Q}$ are introduced for a certain configuration $\tilde{\mathbf{x}}$, *i.e.* in general the second derivative matrix will be diagonal only at this point. Therefore we have

$$H_{\mathrm{mol}} = \sum_{a=1}^{N_{\mathrm{rc}}} T_a + V_{\mathrm{ref}}(\mathbf{x}) + \sum_{k=1}^{N_{\mathrm{sub}}} \left(T_k + \frac{1}{2}\omega_k^2(\mathbf{x})Q_k^2\right) - \sum_{k=1}^{N_{\mathrm{sub}}} \left[\left(f_k(\mathbf{x}) - \frac{1}{2}\sum_{l\neq k=1}^{N_{\mathrm{sub}}} K_{kl}(\mathbf{x})Q_l\right)Q_k\right]. \quad (2)$$

Note that there are N_{rc} reaction coordinates and therefore $N_{\mathrm{sub}} = 3N_{\mathrm{nuc}} - N_{\mathrm{rc}} - 6$ substrate normal modes. The kinetic energy operator for the reaction and substrate coordinates has been introduced as $T_a = P_a^2/2M_a$ and $T_k = P_k^2/2$, respectively.

There are two types of couplings between the reaction coordinate and the substrate normal modes. First, because the reaction coordinate does not necessarily follow a minimum energy path, a force $f_k(\mathbf{x})$ is acting on the normal modes. Second, there is a coupling between different normal modes mediated by the reaction coordinate $K_{kl}(\mathbf{x})$ $(k \neq l)$, note that $K_{kl}(\mathbf{x}) = K_{lk}(\mathbf{x})$. If the latter coupling is weak, it is reasonable to introduce the normal mode frequency $\omega_k^2(\mathbf{x}) \equiv K_{kk}(\mathbf{x})$. The strength of the linear coupling can also be expressed in terms of the

reorganization energy, that is the energy which is required to restore the equilibrium position of the substrate oscillators if the off-diagonal elements of the force constant matrix are neglected:

$$E_{\mathrm{reorg}}(\mathbf{x}) = \sum_{k=1}^{N_{\mathrm{sub}}} \Delta_k(\mathbf{x}) = \sum_{k=1}^{N_{\mathrm{sub}}} \frac{f_k^2(\mathbf{x})}{2\omega_k^2(\mathbf{x})}\,. \tag{3}$$

The interaction of the molecule with the laser field is treated in semiclassical dipole approximation, *i.e.* the interaction Hamiltonian is

$$H_{\mathrm{F}}(\mathbf{x},t) = -\mu(\mathbf{x})\mathcal{E}(t), \tag{4}$$

where $\mu(\mathbf{x})$ is the dipole moment function. In principle the dipole moment variation along the normal modes could also be incorporated, *e.g.* within a linear approximation [43]. However, here we are primarily interested in the excitation of an OH(D) vibration which is the optically active DOF in the considered spectral region. Therefore, $\mathcal{E}(t)$ in equation (4) stands for the component of the electric field strength along the optically active or reaction coordinate.

2.2 TDSCF quantum dynamics

In the TDSCF approach the total wave function $\Psi(x,\{Q_k\},t)$ is written as a Hartree product (note that we restrict ourselves to a single reaction coordinate x in the following, *i.e.* $a = \mathrm{a}$ in Eq. (2))

$$\Psi(x,\{Q_k\},t) = \Psi_{\mathrm{a}}(x,t) \prod_{k=1}^{N_{\mathrm{sub}}} \Psi_k(Q_k,t). \tag{5}$$

Given some Hamiltonian H the TDSCF equations of motion are derived from the Dirac-Frenkel variational principle [28,29]:

$$\langle \delta\Psi | \mathrm{i}\hbar\frac{\partial}{\partial t} - H|\Psi\rangle = 0. \tag{6}$$

After omitting an unimportant phase factor the equation of motion for the reaction coordinate reads

$$\mathrm{i}\hbar\frac{\partial}{\partial t}\Psi_{\mathrm{a}}(x,t) = \left[T_{\mathrm{a}} + V_{\mathrm{SCF}}(x,t) - \mu(x)\mathcal{E}(t)\right]\Psi_{\mathrm{a}}(x,t), \tag{7}$$

where the time-dependent self-consistent field potential $V_{\mathrm{SCF}}(x,t)$ is defined as

$$V_{\mathrm{SCF}}(x,t) = V_{\mathrm{ref}}(x) + \sum_k \left[\frac{1}{2}\omega_k^2(x)\langle\Psi_k|Q_k^2|\Psi_k\rangle - \Big(f_k(x) - \frac{1}{2}\sum_{l\neq k} K_{kl}(x)\langle\Psi_l|Q_l|\Psi_l\rangle\Big)\langle\Psi_k|Q_k|\Psi_k\rangle\right]. \tag{8}$$

For the substrate modes we obtain

$$\mathrm{i}\hbar\frac{\partial}{\partial t}\Psi_k(Q_k,t) = \Big[T_k + \frac{1}{2}\Omega_k^2(t)Q_k^2 - F_k(t)Q_k\Big]\Psi_k(Q_k,t) \tag{9}$$

Here we defined the time-dependent harmonic frequencies

$$\Omega_k^2(t) = \langle\Psi_{\mathrm{a}}|\omega_k^2(x)|\Psi_{\mathrm{a}}\rangle \tag{10}$$

and the time-dependent intramolecular linear driving forces

$$F_k(t) = \langle\Psi_{\mathrm{a}}|f_k(x)|\Psi_{\mathrm{a}}\rangle - \frac{1}{2}\sum_{l\neq k}\langle\Psi_{\mathrm{a}}|K_{kl}(x)|\Psi_{\mathrm{a}}\rangle\langle\Psi_l|Q_l|\Psi_l\rangle. \tag{11}$$

The equations of motion (9) are of the form of linearly driven harmonic oscillators with time-dependent frequencies. The corresponding analytical solutions are well-known (see, for example, Refs. [44–46]). Therefore, all time-dependent expectation values such as $\langle\Psi_k(t)|Q_k|\Psi_k(t)\rangle$ and $\langle\Psi_k(t)|Q_k^2|\Psi_k(t)\rangle$ as well as the vibrational state populations (see below), are reduced to tabulated integrals [47].

Initially all DOF are assumed to be in the respective vibrational ground states. The "true" eigenfunction of the vibrational ground state of the overall molecular system has been obtained by the relaxation method [48], *i.e.* by propagating the TDSCF equations of motion in imaginary time, with the laser field being switched off, $\mathcal{E}(t) = 0$. This gives the stationary vibrational ground states $|\Psi_{\mathrm{a},g}\rangle$ and $|\Psi_{k,g}\rangle$ corresponding to the overall vibrational ground state $|\Psi_g\rangle$ of the entire molecule. It is represented by the wave function

$$\Psi_g(x,\{Q_k\}) = \Psi_{\mathrm{a},g}(x) \prod_{k=1}^{N_{\mathrm{sub}}} \Psi_{k,g}(Q_k). \tag{12}$$

This state is then used as the initial state for the simulations of the laser-driven molecular dynamics accompanied and followed by intramolecular vibrational energy redistribution (IVR).

As a basis set for the reaction coordinate use is made of the eigenstates supported by the time-independent self-consistent field potential $V_g^{\mathrm{SCF}}(x)$ corresponding to the overall ground vibrational state (12), that is,

$$V_g^{\mathrm{SCF}}(x) = V_{\mathrm{ref}}(x) + \sum_k \Big\{\frac{1}{2}\omega_k^2(x)\langle\Psi_{k,g}|Q_k^2|\Psi_{k,g}\rangle - \Big[f_k(x) - \frac{1}{2}\sum_{l\neq k} K_{kl}(x)\langle\Psi_{l,g}|Q_l|\Psi_{l,g}\rangle\Big]\langle\Psi_{k,g}|Q_k|\Psi_{k,g}\rangle\Big\}. \tag{13}$$

The respective eigenfunctions $\psi_{\mathrm{a},v}^{\mathrm{SCF}}(x)$ are derived from the eigenvalue equation

$$\left[T_{\mathrm{a}} + V_g^{\mathrm{SCF}}(x)\right]\psi_{\mathrm{a},v}^{\mathrm{SCF}}(x) = E_{\mathrm{a},v}^{\mathrm{SCF}}\,\psi_{\mathrm{a},v}^{\mathrm{SCF}}(x) \tag{14}$$

which has been solved by the Fourier grid Hamiltonian method [49].

For the substrate modes the time-dependent self-consistent field basis set, $\psi_{k,v}^{\mathrm{SCF}}(Q_k,t)$ is used, with the instantaneous eigenfunctions following from the eigenvalue

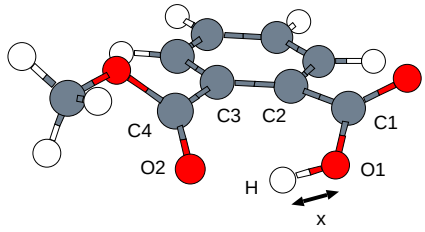

Fig. 1. Equilibrium geometry of phthalic acid monomethylester as obtained by using the MP2 method and a 6-31+G(d, p) basis set. The reaction coordinate x is taken to coincide with the bond distance $R_{\mathrm{O1-H}}$.

equations

$$\left[T_k + \frac{1}{2}\Omega_k^2(t)Q_k^2\right]\psi_{k,v}^{\mathrm{SCF}}(Q_k,t) = E_{k,v}^{\mathrm{SCF}}(t)\,\psi_{k,v}^{\mathrm{SCF}}(Q_k,t). \tag{15}$$

The parametric dependence on time comes from the time-dependent harmonic frequencies $\Omega_k(t)$ defined by equation (10). The eigenfunctions $\psi_{k,v}^{\mathrm{SCF}}(Q_k,t)$ are the well-known harmonic oscillator wave functions. In principle there would have been at least two other choices for the basis set describing the substrate modes, *i.e.* either a constant Hamiltonian or a Hamiltonian which includes the driving force $F_k(t)$. Since it is primarily the driving force whose effect on the oscillator dynamics shall be studied, the basis set defined through equation (15) appears to be most suitable. In Section 3.2 we will monitor IVR dynamics by calculating the time-dependent populations which follow from projection of the wave functions $\Psi_{\mathrm{a}}(t)$ and $\Psi_k(t)$ on the SCF vibrational eigenstates.

3 Results

3.1 Model system

In the following we will consider the OH(D) stretching dynamics in the strong intramolecular hydrogen bond formed in PMME-H (-D). This choice has been motivated by the recent IR pump-probe observation of vibrational quantum beats for this system [25].

We performed *ab initio* quantum chemical calculations [50] to determine the most stable geometry and subsequently the CRS Hamiltonian according to equation (2). From the quantum chemical point of view the study of hydrogen bonds necessitates the inclusion of dynamic correlation effects. This means that one should use, for instance, second order Møller-Plesset perturbation theory (MP2) or alternatively the computationally less demanding Density Functional Theory (DFT) (for a comparison see also Ref. [51]). In Figure 1 we show the equilibrium geometry of PMME following from an MP2 calculation with a 6-31+G(d, p) basis set. Note that the molecule is not planar, the symmetry group is only C_1.

Concerning the structure two points are worth mentioning: first, there exist several although higher energetic isomers, *e.g.* a hydrogen-bonded rotamer with respect to the ester group[1]. Second, using DFT with the B3LYP functional one obtains a minimum configuration (see also [25]) which is slightly different from the MP2 data, see Table 1. Basically, the DFT predicts a more planar structure as compared with the MP2 method.

Table 1. Equilibrium bond lengths and angles for the most stable isomer of PMME-H as obtained on the MP2 and DFT/B3LYP level of theory (only the most relevant differences are reported, bond lengths are given in Å).

		MP2	DFT/B3LYP
bonds	H–O1	0.983	0.992
	O1–C1	1.343	1.330
	C1–C2	1.518	1.534
	C3–C4	1.488	1.494
	C4–O2	1.235	1.229
	O2–H	1.702	1.593
angles	H–O1–C1	111.2	112.4
	O1–C1–C2	119.4	120.2
	C1–C2–C3	128.0	129.8
	C2–C3–C4	124.2	124.9
	C3–C4–O2	125.4	125.9
dihedrals	H–O1–C1–C2	−9.4	−8.3
	O1–C1–C2–C3	**38.9**	**25.3**
	O2–C4–C3–C2	−37.1	**−23.8**

Being interested in the dynamics of the OH stretching vibration the natural choice of the reaction coordinate is the bond length $R_{\mathrm{O1-H}}$, see Figure 1[2]. We will choose the coordinate system such that the x-direction points along the OH bond in the equilibrium configuration, *i.e.* $\mathbf{x} = (x \equiv R_{\mathrm{O1-H}}, y = 0, z = 0)$. This restriction of the hydrogen motion is motivated by the fact that there is a normal mode corresponding to an almost pure OH stretching vibration. The reference geometry for the substrate $\mathbf{Z}^{(0)}$ is taken to be the equilibrium configuration (see Fig. 1) corresponding to the equilibrium bond length $x_{\mathrm{eq}} = 0.983$ Å. This configuration has also been used for determination of the $N_{\mathrm{sub}} = 54$ normal modes, *i.e.* $\tilde{x} = x_{\mathrm{eq}}$.

In Figure 2 we show the reference potential $V_{\mathrm{ref}}(x)$ for the motion of the hydrogen atom together with the three lowest eigenfunctions as calculated using the Fourier grid method [49]. The potential has the form typical for strong hydrogen bonds [11]. It is rather anharmonic and in fact already the 0→1 vibrational transition frequency is 200 cm^{-1} below the value obtained with harmonic approximation in the vicinity of the equilibrium. We further notice that upon 0→1 excitation the dynamics will take place within a range of ±0.3 Å with respect to the potential minimum.

Analyzing the forces and reorganization energies of the substrate normal modes in this region we found that there are several low frequency modes (below 300 cm^{-1})

[1] There is also an isoenergetic enantiomer, but separated by a rather high barrier from the structure in Figure 1. Thus, mutual coupling can be neglected.

[2] Strictly speaking this is no true "reaction coordinate" since we are considering a nonreactive process.

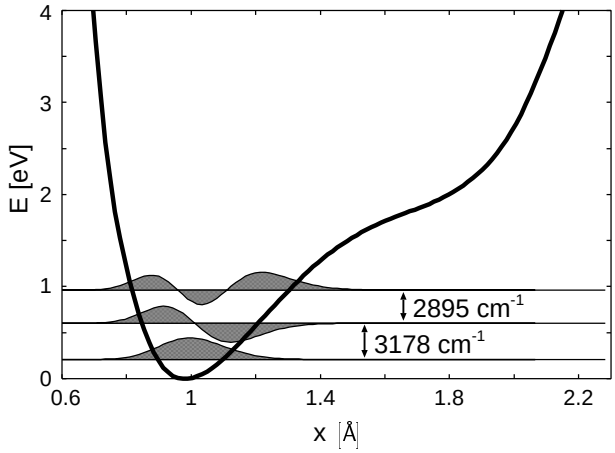

Fig. 2. Reference potential for motion of the hydrogen atom along the one-dimensional reaction coordinate as obtained from the MP2 calculation. Also shown are the three lowest vibrational eigenfunctions for this potential vertically displaced, according to the respective eigenenergies.

which couple to the reaction coordinate. The largest coupling in this frequency range is experienced by the lowest-frequency mode $\nu_{54} = 68$ cm^{-1}. The displacement vectors shown in Figure 3 indicate that this is a rather delocalized mode which, by virtue of a rotation type vibration of the ester group, modifies the distance $R_{\mathrm{O1-O2}}$ between the heavy atoms participating in the hydrogen bond. Interestingly, the most strongly coupled mode has a much higher frequency, $\nu_{28} = 1082$ cm^{-1}. As can be seen in Figure 4 this mode is more localized at the hydrogen bond. In particular it involves a kind of out-of-plane motion of O1, supporting the notion of its strong effect on the hydrogen bond. Figures 3 and 4 also show the diagonal elements of the second derivative matrix, *i.e.* the approximate frequencies, and the forces (as obtained from the gradients of the potential) acting on the two modes. We notice that mode ν_{28} not only experiences an appreciable force in the vicinity of the minimum configuration but also its frequency changes rather strongly. In fact the magnitude of both quantities rises dramatically when moving to smaller distances. This indicates that most likely the harmonic approximations breaks down in this region of the PES, which fortunately is not accessed during our dynamics simulations. A possible explanation for this breakdown of the harmonic approximation could be that the normal mode displacement vectors in Figure 4A roughly point towards the hydrogen atom. This reasoning is supported by the rather similar behavior which is found for the low-frequency mode ν_{54}, but now at large distances, see Figure 3.

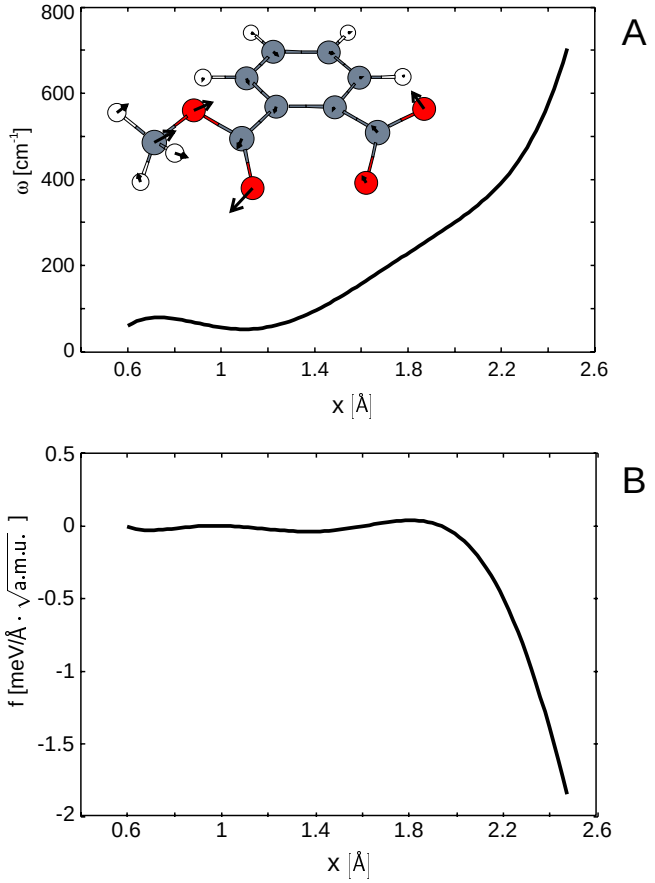

Fig. 3. Frequency (A) and force (B) for mode ν_{54}, the most strongly coupled low-frequency mode in the vicinity of the equilibrium geometry. The displacement vectors shown in the inset of panel (A) indicate that this mode is of rotation type with respect to the ester group.

3.2 Dynamics

3.2.1 Numerical implementation

The TDSCF equation for the reaction coordinate (7) has been treated by representing wave function and operators on a 256 point spatial grid ranging from $x_{\min} = 0.3$ Å to $x_{\max} = 3.0$ Å. The time propagation has been accomplished by the split-operator method [52,53], with the fast Fourier transform procedure used to obtain the spatial derivatives. The time step of propagation Δt ranged from 0.1 to 0.5 a.t.u.

At large values of x, absorbing boundary conditions were employed. Specifically, we used the smooth imaginary optical potential $U_{\mathrm{op}}(x)$, where

$$U_{\mathrm{op}}(x) = -\mathrm{i}U_0 \exp\left\{(3/2)\left[1 - \frac{(x_{\max} - x_{\mathrm{op}})^2}{(x - x_{\mathrm{op}})^2}\right]\right\}, \quad (16)$$

if $x \geq x_{\mathrm{op}}$ and $U_{\mathrm{op}}(x) = 0$ otherwise (for further details see Ref. [54] and references therein). The results presented below have been calculated for $U_0 = 0.1E_{\mathrm{h}}$ and $x_{\mathrm{op}} = 2.4$ Å. In practice, however, the wave packets never approached the outer boundary of the x interval.

Concerning the equations for the substrate modes (9) analytical solutions have been used (see above). This increases remarkably the efficiency of the numerical calculation. The propagation of the 55 dimensional wave function for one picosecond required approximately one hour of CPU-time on a HP-J2240 workstation.

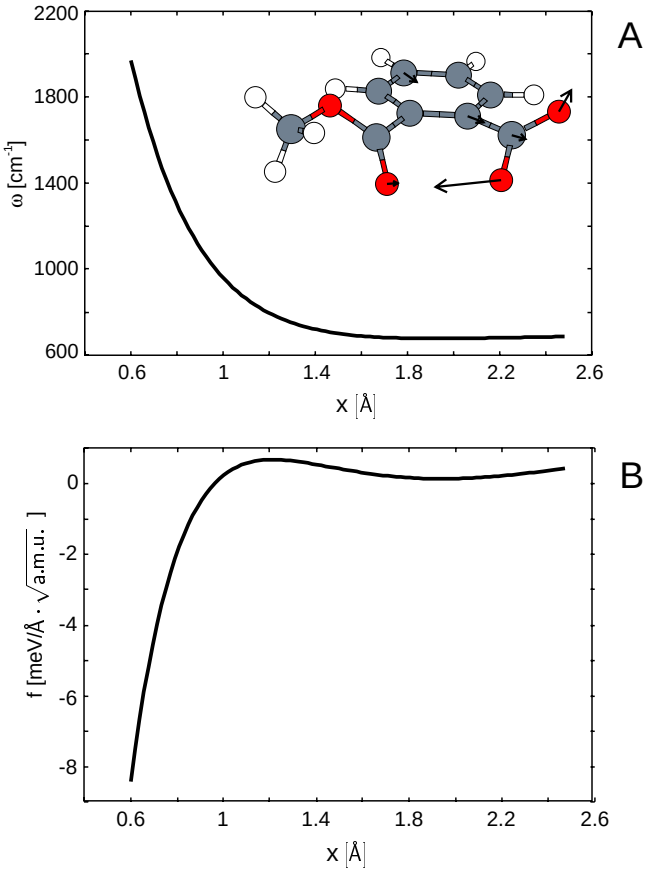

Fig. 4. Frequency (A) and force (B) for the substrate mode ν_{28} which is most strongly coupled to the reaction coordinate. The displacement vectors shown in the inset of panel (A) indicate that for this rather localized mode, O1 moves almost perpendicular to the paper plane.

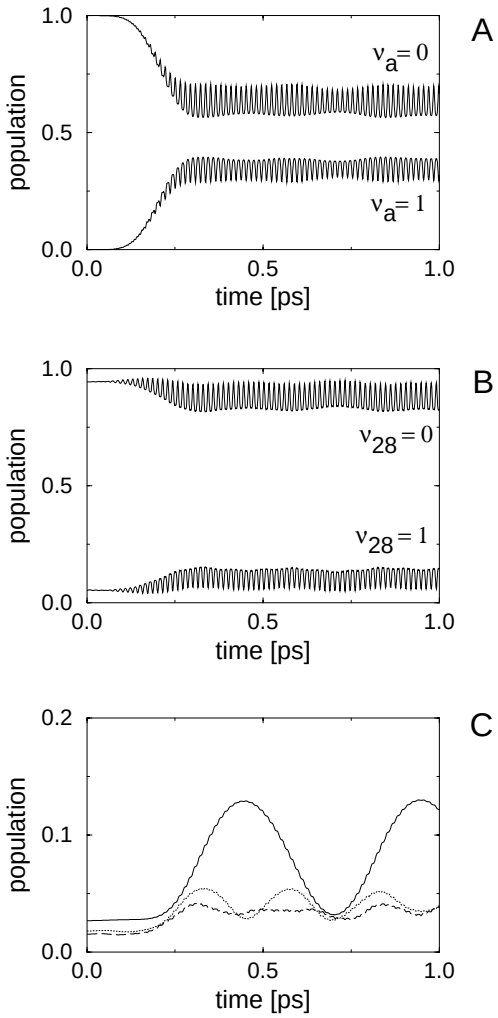

Fig. 5. Population dynamics according to equations (18, 19) for PMME-D upon excitation with a pulse of the form (17) with $\mathcal{E}_0 = 0.005$ a.u., $\tau = 330$ fs, and $\omega = 2375$ cm^{-1}, panel (A): reaction coordinate, panel (B): mode 28 (see Fig. 4), panel (C): population of the first excited state of modes 54 (solid, see Fig. 3), 52 (dotted), and 50 (dashed). Note that the finite populations of the first excited oscillator states at time zero are due to the driving force which is averaged with respect to the full ground state wave function.

In the following we will present results for the population dynamics of the SCF zeroth-order states as defined in equations (18, 19) for PMME-H and its isotope PMME-D. The external field has been chosen to have the form

$$\mathcal{E}(t) = \mathcal{E}_0 \sin^2\left(\frac{t\pi}{\tau}\right)\cos(\omega t). \qquad (17)$$

The carrier frequency was taken such as to give maximum excitation of the 0→1 transition for the SCF reaction coordinate states for $\tau = 330$ fs (full width at half maximum 165 fs) and a given amplitude $\mathcal{E}_0$. In fact the oscillation patterns which will be discussed below are not very sensitive to the actual value of $\mathcal{E}_0$ (within reasonable limits). Over a wide range of field strengths only the magnitude of the quantum beats is affected.

3.2.2 1D zeroth-order states

In the following we will focus on the populations of the one-dimensional (1D) zeroth-order states defined by equations (14, 15), *i.e.* for the reaction coordinate we have

$$P_{\mathrm{a},v}(t) = |\langle \psi^{\mathrm{SCF}}_{\mathrm{a},v} | \Psi_{\mathrm{a}}(t) \rangle|^2 \qquad (18)$$

and for the different substrate normal modes it is

$$P_{k,v}(t) = |\langle \psi^{\mathrm{SCF}}_{k,v} | \Psi_k(t) \rangle|^2. \qquad (19)$$

The time-dependent populations given in equations (18, 19) are presented in Figure 5 for PMME-D and in Figure 6 for PMME-H (for pulse parameters see figure captions).

Comparing both figures we notice that the principal behavior does not change appreciably upon H/D substitution. The populations of the two lowest SCF states along the reaction coordinate show rapid oscillations modulated by several slower oscillations, panel (A) of Figures 5 and 6. Inspecting the dynamics of the most strongly coupled mode ν_{28} in panels (B) we find a rather similar behavior. It should be noted again that there is no direct excitation

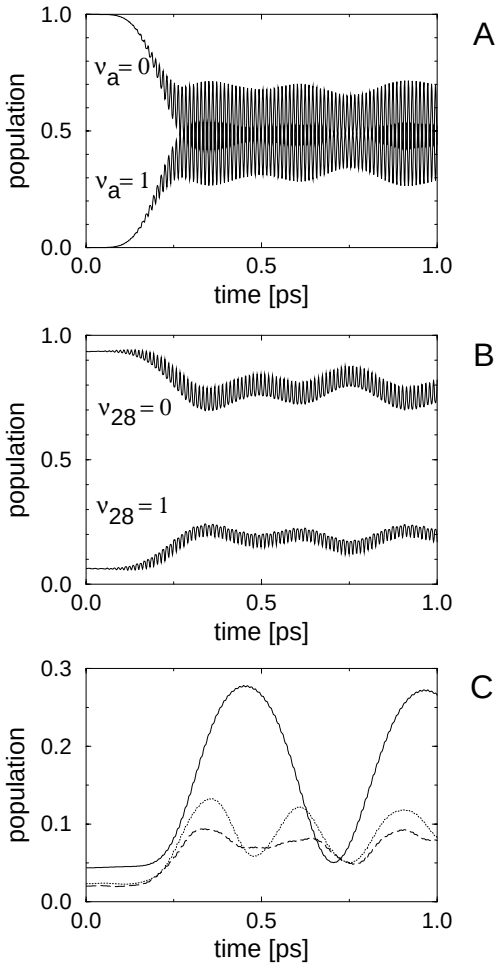

Fig. 6. Population dynamics according to equations (18, 19) for PMME-H upon excitation with a pulse of the form (17) with $\mathcal{E}_0 = 0.004$ a.u., $\tau = 330$ fs, and $\omega = 3150$ cm^{-1}, panel (A): reaction coordinate, panel (B): mode 28 (see Fig. 4), panel (C): population of the first excited state of modes 54 (solid, see Fig. 3), 52 (dotted), and 50 (dashed).

of the substrate oscillators, *i.e.* the nonequilibrium populations are entirely caused by the intramolecular driving force $F_k(t)$ given by equation (11). The fast oscillations can therefore be understood in terms of the well-known dynamics [11] of two states (here ($\nu_a = 1$, $\nu_{28} = 0$) and ($\nu_a = 0$, $\nu_{28} = 1$)) which are strongly coupled but have a rather large energy mismatch (in the present case about 2 000 cm^{-1}).

The appearance of low-frequency modulations of the population dynamics in Figures 5 and 6 (panels (A) and (B)), however, follows from the coupling to the various low-frequency normal modes, *e.g.*, mode ν_{54}, Figure 3. In order to support this point we show in panels (C) of Figures 5 and 6 the populations of the first excited vibrational SCF state for several low-frequency modes. The respective ground state populations are out-of phase, higher vibrational states are only negligibly excited. This result indicates that there is substantial IVR into the low-frequency modes with mode ν_{54} playing the dominant role. This renders a detailed analysis of the different low-frequency components observed in the OH(D) population dynamics in Figures 5 and 6 rather difficult, since for N coupled levels there are $N(N-1)/2$ possible beating frequencies, see also reference [10]. Finally, we would like to point out that on the time scale of 2 ps we did not observe any relaxation in the sense that vibrational excitation energy is distributed over all possible substrate modes such that the population of the first excited OH(D) vibrational state effectively decays on some intermediate time scale. In other words, the present situation corresponds to the scenario typical for restricted IVR [9]. Strictly speaking there is of course no true relaxation in this finite dimensional system [11].

3.2.3 3D zeroth-order states: in-phase and out-of-phase oscillations

The characteristic feature of IVR are quantum beat patterns represented by *in-phase* and *out-of-phase* oscillations of populations, which clearly indicate those vibrational states, or groups of states (manifolds), between which the intramolecular vibrational energy exchange takes place [3,9,10] (see also reference [55,56]). However, inspection of the 1D SCF populations in Figures 5 and 6 does not provide an obvious picture in this respect. That's why in the following we will comprise the information contained in the populations of the states for the reaction coordinate and the strongly coupled modes ν_{28} and ν_{54} to obtain a better understanding of the IVR process in PMME-D.

Let us consider the populations of 3D zeroth-order states, which represent non-stationary molecular states with explicitly given excitation in the chosen DOF. Within the TDSCF approach such a state can be defined as a product of the respective 1D zeroth-order states. For the considered three mode case the 3D zeroth-order states are represented by the three ordered quantum numbers (v_1, v_2, v_3), indicating v_1 vibrational quanta in the reaction coordinate, v_2 and v_3 vibrational quanta in the substrate mode ν_{28} and ν_{54}, respectively. The time-dependent populations of these 3D zeroth-order states will be denoted as $P_{v_1,v_2,v_3}(t)$ and calculated as follows:

$$P_{v_1,v_2,v_3}(t) = P_{\mathrm{a},v_1}(t)\, P_{28,v_2}(t)\, P_{54,v_3}(t). \qquad (20)$$

The energy level diagram for the 3D zeroth-order states is shown in Figure 7A. The actual advantage of this approach comes with the combination of groups of states into state manifolds. We will call the M_n manifold the collection of 3D zeroth-order states with n vibrational quanta in the reaction coordinate but excluding the state $(n, 0, 0)$, see Figure 7A.

Let us discuss the population dynamics of the previous section in terms of the 3D zeroth-order states and the different state manifolds. In Figure 8A the short-term dynamics of the state $(1, 0, 0)$ and the manifold M_0 is shown for the first 500 femtoseconds. Clearly, the oscillations are in-phase and out-of-phase with respect to each other. This is indicative of energy exchange between the first excited

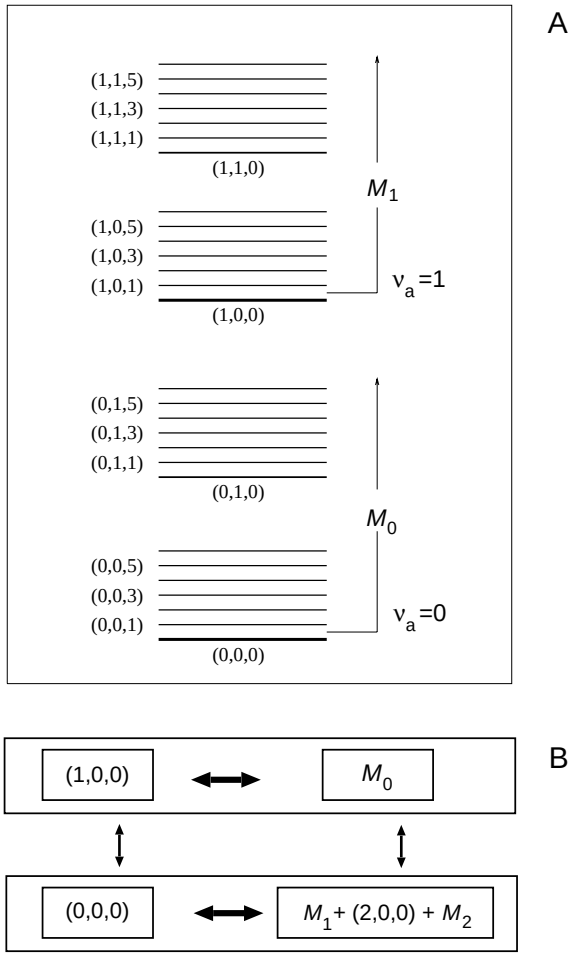

Fig. 7. (A) Level scheme for grouping of 3D zeroth-order states $(\nu_a, \nu_{28}, \nu_{54}) \equiv (v_1, v_2, v_3)$ into state manifolds M_n. Note that the states $(n, 0, 0)$ are excluded from M_n. (B) States and manifolds between which energy exchange takes place (see text).

state of the OD stretching vibration and the substrate states which build on the OD ground state. In panel (B) of Figure 8 we find the same type of in-phase and out-of-phase oscillations between the ground state $(0, 0, 0)$ and the combination of states $[M_1 + (2, 0, 0) + M_2]$. Closer inspection shows that the in-phase and out-of-phase beating patterns in Figures 8A and 8B are not perfect. This indicates energy exchange between the two enlarged manifolds, $[(0, 0, 0) + M_1 + (2, 0, 0) + M_2]$ and $[M_0 + (1, 0, 0)]$, which also proceeds *via* in-phase and out-of-phase oscillations as can be seen in panel (C) of Figure 8. As a note in caution we would like to point out that not all the states in the manifolds are equally important.

Next we focus on the slow oscillations seen for the 3D population dynamics on a longer time scale of 2 picoseconds in panel (D) of Figure 8. First, we notice that the slow oscillations of the optically "active" states, *i.e.* $(0, 0, 0)$ and $(1, 0, 0)$, proceed in-phase with each other. The slow oscillations of the populations of both states, however, are out-of-phase with the manifold M_0. The overall population of the M_0 manifold is for the most part the sum of slowly oscillating population of state $(0, 0, 1)$, which defines the envelope of this manifold's population dynamics, and the fast oscillating population of state $(0, 1, 0)$. In fact the 3D state $(0, 1, 0)$ represents the fast oscillating 1D zeroth-order state $|\psi^{\rm SCF}_{k=28,v=1}\rangle$ while the 3D state $(0, 0, 1)$ represents the slowly oscillating 1D state $|\psi^{\rm SCF}_{k=54,v=1}\rangle$ (*cf.* Fig. 5). The overall picture of the IVR dynamics which follows from this analysis in sketched in Figure 7B.

3.2.4 Transient absorption spectroscopy

In the following we would like to answer the question, how the population dynamics discussed so far is reflected in pump-probe nonlinear optical spectroscopy of the OH band of PMME-H. To this end we have calculated the energy which is absorbed by a weak probe pulse from the state prepared by the pump pulse. We define the transient absorption signal as

$$S(\tau_{\rm del}) = \langle H_{\rm mol}\rangle_{\rm pump+probe} - \langle H_{\rm mol}\rangle_{\rm pump}\ , \qquad (21)$$

where $\langle H_{\rm mol}\rangle$ denotes the expectation value of energy after the action of the pulses and for a given delay time $\tau_{\rm del}$ between pump and probe pulse. Note that the signal defined by equation (21) does not correspond to the signal measured in a third-order pump-probe experiment in the spatial direction of the probe pulse propagation. In fact the present calculation includes the laser field nonperturbatively and we do not keep track of the phase of the polarization, *i.e.* in this sense $S(\tau_{\rm del})$ is proportional to the signal which would be obtained by integrating over all spatial directions. Several methods have been suggested to solve this problem, *e.g.*, by means of a plane wave type expansion of some appropriately defined density operator [57] or by multiple propagation [58]. In view of the numerical effort connected with the propagation of the present 55-dimensional wave function, these approaches appear to be too demanding. Nevertheless equation (21) provides very useful information as can be seen in Figure 9. Here, the probe pulse has been chosen close to resonance with the 1→2 transition along the reaction coordinate, *i.e.* we have the situation of excited state absorption.

The quantum beats observed in the population dynamics in Figure 6 show up as quasi-periodic modulations of the pump-probe absorption signal. In particular we find the slow oscillations related to the excitation of mode ν_{54}. Note that due to the finite finite duration of the probe pulse, the fast oscillations coming from the coupling between the reaction coordinate and mode ν_{28} cannot be resolved.

4 Summary

The ultrafast dynamics of a strong hydrogen bonded system has been investigated. To our knowledge this presents the first application of a reaction surface Hamiltonian to study the quantum dynamics of such a large molecule in full dimensionality.

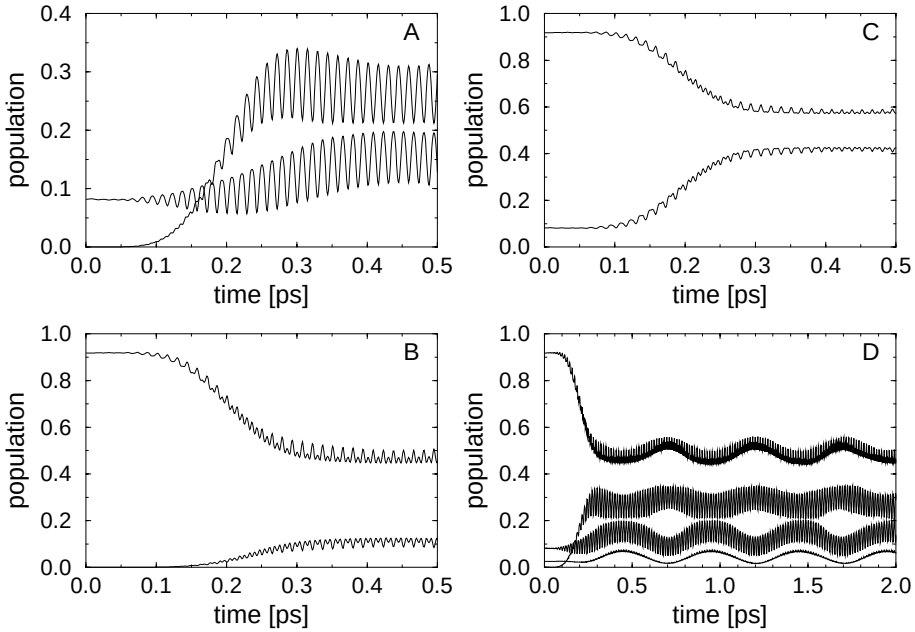

Fig. 8. Population dynamics of 3D zeroth-order states and state manifolds as defined in Figure 7. (A): $(1,0,0)$ and M_0, (B): $(0,0,0)$ and $M_1+M_2+(2,0,0)$, (C): $M_1+M_2+(0,0,0)+(2,0,0)$ and $M_0+(1,0,0)$, (D): $(0,0,0)$, $(1,0,0)$, M_0, and $(0,0,1)$. The order corresponds to the ordering of the curves from top to bottom at the end of the time interval.

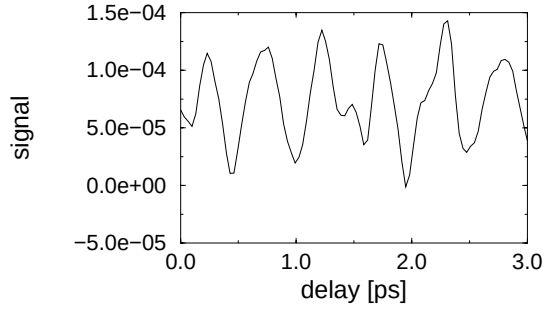

Fig. 9. Transient absorption signal according to equation (21) for excitation in the OH band at 3 150 $cm^{-1}$and detection at 2 750 cm^{-1}, other parameters as in Figure 6, the amplitude of the probe pulse a factor 20 smaller than that of the pump pulse. Note that for strong field driving the signal depends on the relative phase between pump and probe pulse. This effect has been minimized in the present case (actual phase difference is zero) by choosing pump and probe frequencies being resonant to different transitions.

From the analysis of the laser driven populations of the SCF vibrational states for the different DOF we can draw the following conclusions: (i) upon excitation of the optically active reaction coordinate a number of substrate modes are driven out of their equilibrium due to intramolecular forces, see Figures 5 and 6. It should be emphasized that this is a consequence of the anharmonicities contained in the reaction surface Hamiltonian. No such effects would be observed within the harmonic approximation. (ii) The two modes which are most strongly affected correspond to normal mode vibrations which involve the heavy atoms of the hydrogen bond, see Figures 3 and 4. (iii) These two modes are also mainly responsible for the quantum beats observed for the populations of the reaction coordinate vibrational states. (iv) Grouping the different vibrational states into manifolds within a 3D zeroth-order state space enabled us to analyze the beating patterns in terms of intramolecular energy redistribution processes, revealed in the in-phase and out-of-phase population oscillations. The pronounced low-frequency modulation of the populations of the OH(D) stretch SCF vibrational states are mostly due to the lowest-frequency mode. (v) PMME-H and its isotope PMME-D show approximately the same dynamical features which results from the fact, that the coupling to the important substrate modes does not change. (vi) On the time scale of 2 picoseconds we observed no signatures of relaxation type effects.

Finally, we would like to comment on the validity of the TDSCF approach which is the basis for these findings. It is well appreciated that the single configuration treatment performs well as long as details of the mode coupling are only of minor importance [32–34]. Intuitively we would expect that for the present single minimum potential and under low excitation conditions where only the region around the potential minimum is explored (*cf.* Fig. 2) the TDSCF approach is well justified. Indeed preliminary multiconfiguration TDSCF calculations including the ten most strongly coupled degrees of freedom support this point of view.

The oscillations due to the lowest-frequency mode observed for the population dynamics are also present in transient absorption spectra, see Figure 9. This is rather encouraging since our study was motivated by the observation of vibrational quantum beats for this system [25]. Although the agreement in the oscillation periods,

here 500 fs and 300 fs in the experiment, is rather encouraging (a difference is to be expected since accurate quantum chemical determination of low frequencies remains to be a challenge), we would like to point out that at the present we did not aim at simulating the experimental conditions of reference [25]. This would require to take into account the effect of the solvent which leads to a rather rapid relaxation and energy dissipation.

Future work shall be directed towards an approximate inclusion of an environment either within a full-dimensional description or in the spirit of the reduced density matrix approach [11]. It should be pointed out that the present form of the CRS Hamiltonian is well suited to introduce a spectral density for the substrate modes and to apply numerical path integral techniques [59,60]. On the other hand, one could make use of the TDSCF idea in the context of the density matrix dynamics as proposed (on a multiconfiguration level) in reference [61]. Finally, the limits of the single configuration TDSCF theory should be fully explored by using a multiconfiguration approach [32,34].

The authors gratefully acknowledge stimulating discussions with J. Dreyer, T. Elsaesser, P. Hamm, D. Madsen, E. Nibbering, and J. Stenger (Max Born Institut, Berlin) and J. Manz (FU Berlin). G.K. Paramonov wishes to thank the Alexander von Humboldt-Stiftung for the generous support through the Humboldt Research Award. This work has been supported by the Deutsche Forschungsgemeinschaft (Sfb450).

References

1. J. Chaiken, M. Gurnick, J.D. McDonald, J. Chem. Phys. **74**, 106 (1981).
2. W.R. Lambert, P.M. Felker, A.H. Zewail, J. Chem. Phys. **75**, 5958 (1981).
3. P.M. Felker, A.H. Zewail, Phys. Rev. Lett. **53**, 501 (1984).
4. P.G. Smith, J.D. McDonald, J. Chem. Phys. **92**, 1004 (1990).
5. M. Gruebele, Proc. Natl. Acad. Sci. USA **95**, 5965 (1998).
6. M. Bixon, J. Jortner, J. Chem. Phys. **48**, 715 (1968).
7. M. Gruebele, R. Bigwood, Int. Rev. Phys. Chem. **17**, 91 (1998).
8. T. Uzer, Phys. Rep. **199**, 73 (1991).
9. N. Bloembergen, A.H. Zewail, J. Phys. Chem. **88**, 5459 (1984).
10. P.M. Felker, A.H. Zewail, J. Chem. Phys. **82**, 2961 (1985).
11. V. May, O. Kühn, *Charge and Energy Transfer Dynamics in Molecular Systems* (Wiley–VCH, Berlin, 2000).
12. *Proton transfer in hydrogen–bonded systems*, edited by T. bountis (Plenum Press, New York, 1992).
13. *Theoretical Treatments of Hydrogen Bonding*, edited by D. Hadži (Wiley, Chichester, 1997).
14. *Hydrogen Transfer: Experiment and Theory*, edited by H.-H. Limbach, J. Manz, Ber. Bunsenges. Phys. Chem, Vol. 102 (1998).
15. T. Elsaesser, in *Femtosecond Chemistry*, edited by J. Manz, L. Wöste (Verlag Chemie, Weinheim, 1995), Vol. 2, p. 563.
16. A. Douhal, S.K. Kim, A.H. Zewail, Nature **378**, 260 (1995).
17. A. Douhal, F. Lahmani, A.H. Zewail, Chem. Phys. **207**, 477 (1996).
18. S. Takeuchi, T. Tahara, J. Phys. Chem. A **102**, 7740 (1998).
19. P.F. Barbara, P.K. Walsh, L.E. Brus, J. Phys. Chem. **93**, 29 (1989).
20. C. Chudoba, E. Riedle, M. Pfeiffer, T. Elsaesser, Chem. Phys. Lett. **263**, 622 (1996).
21. S. Lochbrunner, A.J. Wurzer, E. Riedle, J. Chem. Phys. **112**, 10699 (2000).
22. S. Woutersen, U. Emmerichs, H.J. Bakker, Nature **278**, 658 (1997).
23. H.-K. Nienhuys, S. Woutersen, R.A. van Santen, H.J. Bakker, J. Chem. Phys. **111**, 1494 (1999).
24. R. Laenen, K. Simeonides, J. Phys. Chem. A **102**, 7207 (1998).
25. J. Stenger, D. Madsen, J. Dreyer, E.T.J. Nibbering, P. Hamm, T. Elsaesser, in *Ultrafast Phenomena XII*, edited by T. Elsaesser, S. Mukamel, M. Murnane, N. Scherer (Springer, New York, 2000), Springer Series in Chemical Physics, p. 542.
26. W.H. Miller, N.C. Handy, J.E. Adams, J. Chem. Phys. **72**, 99 (1980).
27. R.B. Gerber, V. Buch, M.A. Ratner, J. Chem. Phys. **77**, 3022 (1982).
28. P.A.M. Dirac, Proc. Cambr. Philos. Soc. **26**, 376 (1930).
29. J. Frenkel, *Wave Mechanics* (Clarendon Press, Oxford, 1934).
30. P. Jungwirth, R.B. Gerber, Chem. Rev. **99**, 1583 (1999).
31. W.H. Miller, in *Stochasticity and Intramolecular Redistribution of Energy*, edited by R. Lefebvre, S. Mukamel (D. Reidel Publishing Company, Dordrecht, 1987), Vol. 200 of NATO ASI Series, p. 263.
32. N. Makri, W.H. Miller, J. Chem. Phys. **87**, 5781 (1987).
33. S. Hammes-Shiffer, Faraday Disc. **110**, 391 (1998).
34. M.H. Beck, A. Jäckle, G.A. Worth, H.-D. Meyer, Phys. Rep. **324**, 1 (2000).
35. *The hydrogen bond theory*, edited by P. Schuster, G. Zundel, C. Sandorfi (North-Holland, Amsterdam, 1976).
36. K. Fukui, J. Phys. Chem. **74**, 4161 (1970).
37. S. Kato, H. Kato, K. Fukui, J. Am. Chem. Soc. **99**, 684 (1977).
38. T. Carrington, W.H. Miller, J. Chem. Phys. **81**, 3941 (1984).
39. N. Shida, P.F. Barbara, J.E. Almlöf, J. Chem. Phys. **91**, 4061 (1989).
40. B.A. Ruf, W.H. Miller, J. Chem. Soc. Faraday Trans. 2 **84**, 1523 (1988).
41. A.E. Orel, O. Kühn, Chem. Phys. Lett. **304**, 285 (1999).
42. H. Naundorf, J.A. Organero, A. Douhal, O. Kühn, J. Chem. Phys. **110**, 11286 (1999).
43. A.E. Orel, Y. Zhao, O. Kühn, J. Chem. Phys. **112**, 94 (2000).
44. K. Husimi, Prog. Theor. Phys. **9**, 381 (1953).
45. P. Pechukas, J.C. Light, J. Chem. Phys. **44**, 3897 (1966).
46. X. Chapusiat, J. Manz, Mol. Phys. **26**, 1577 (1973).
47. I.S. Gradshteyn, I.M. Ryzhik, *Tables of Integrals, Series, and Products* (Academic Press, New York, 1980).
48. R. Kosloff, H. Tal-Ezer, Chem. Phys. Lett. **127**, 223 (1986).

49. C.C. Marston, G.G. Balint-Kurti, J. Chem. Phys. **91**, 3571 (1989).
50. M.J. Frisch, G.W. Trucks, H.B. Schlegel, G.E. Scuseria, M.A. Robb, J.R.C.V.G. Zakrzewski, J.A. Montgomery, R.E. Stratmann, J.C. Burant, S. Dapprich, J.M. Millam, A.D. Daniels, K.N. Kudin, M.C. Strain, O. Farkas, J. Tomasi, V. Barone, M. Cossi, R. Cammi, B. Mennucci, C. Pomelli, C. Adamo, S. Clifford, J. Ochterski, G.A. Petersson, P.Y. Ayala, Q. Cui, K. Morokuma, D.K. Malick, A.D. Rabuck, K. Raghavachari, J.B. Foresman, J. Cioslowski, J.V. Ortiz, B.B. Stefanov, G. Liu, A. Liashenko, P. Piskorz, I. Komaromi, R. Gomperts, R.L. Martin, D.J. Fox, T. Keith, M.A. Al-Laham, C.Y. Peng, A. Nanayakkara, C. Gonzalez, M. Challacombe, P.M.W. Gill, B.G. Johnson, W. Chen, M.W. Wong, J.L. Andres, M. Head-Gordon, E.S. Replogle, J.A. Pople, Gaussian 98 (Revision A.6) (Gaussian Inc., Pittsburgh, 1998).
51. N. Došlić, K. Sundermann, L. González, O. Mó, J. Giraud-Girard, O. Kühn, Phys. Chem. Chem. Phys. **1**, 1249 (1999).
52. M.D. Feit, J.A. Fleck, A. Steiger, J. Comp. Phys. **47**, 412 (1982).
53. D. Kosloff, R. Kosloff, J. Comp. Phys. **52**, 35 (1982).
54. M. Kaluža, J.T. Muckerman, P. Gross, H. Rabitz, J. Chem. Phys. **100**, 4211 (1994).
55. G.K. Paramonov, Chem. Phys. Lett. **250**, 505 (1996).
56. M. Oppel, G.K. Paramonov, Appl. Phys. B **71**, 319 (2000).
57. J.Y. Bigot, B. Höhnerlage, Phys. Stat. Sol. (b) **121**, 649 (1984).
58. L. Seidner, G. Stock, W. Domcke, J. Chem. Phys. **103**, 3998 (1995).
59. N. Makri, J. Phys. Chem. A **102**, 4144 (1998).
60. O. Kühn, Eur. Phys. J. D **6**, 49 (1999).
61. A. Raab, I. Burghardt, H.D. Meyer, J. Chem. Phys. **111**, 8759 (1999).